High Power Laser Science and Engineering, (2024), Vol. 12, e54, 12 pages.
doi:10.1017/hpl.2024.39

HIGH POWER LASER SCIENCE AND ENGINEERING

RESEARCH ARTICLE

Tracing the origins of mode coupling for beam quality optimization in high-power fiber laser delivery systems

Xiao Chen[1], Shanmin Huang[1], Liangjin Huang[1,2,3], Lei Du[1], Zhiping Yan[1,2,3], Zhiyong Pan[1,2,3], Pu Zhou[1], and Zongfu Jiang[1,2,3]

[1] *College of Advanced Interdisciplinary Studies, National University of Defense Technology, Changsha, China*

[2] *Nanhu Laser Laboratory, National University of Defense Technology, Changsha, China*

[3] *Hunan Provincial Key Laboratory of High Energy Laser Technology, National University of Defense Technology, Changsha, China*

(Received 25 February 2024; revised 24 May 2024; accepted 17 June 2024)

Abstract

Suppressing mode degradation is the key issue for high-power laser delivery; however, diagnosing mode degradation in its entirety, ranging from the contents and origins to locations, has always been a major obstacle. Here, a versatile approach for tracing the origins of mode coupling is demonstrated through addressing the differential intermodal dispersions of fiber modes. Full recognition for modal contents and the origins of mode degradation are experimentally completed in a two-mode fiber laser delivery system, which assists a significant improvement of beam quality M^2 from 1.35 to 1.15 at the highest power of over 300 W. This method yields a quantitative characterization for manipulating the individual mode of dual-mode coupling origins or their combinations. This work points toward a promising strategy for the online tracing of mode coupling in cascade fiber links, thus enabling further pursuit of seeking extreme beam quality in high-power fiber laser systems.

Keywords: beam quality; intermodal dispersion; laser delivery; mode diagnosis; origins of mode coupling

1. Introduction

Excellent beam quality is constantly pursued for the development of high-power laser technology[1–5]. Normally, a pure modal content implies a smaller value of beam quality factor M^2. It is generally desirable to obtain an output field as close as possible to the pure fundamental mode (LP_{01} mode), that is, the diffraction-limited output. The main origin for beam quality degradation is the mode coupling events in the optical fiber, including distributed mode coupling and discrete mode coupling. The former is a continuous event distributing along the whole length of the fiber, showing primary sensitivity to the inherent defects of the optical fiber, such as fluctuations of the refractive index of the core dimension. The latter is a discrete event, mainly determined by the excitation state of the launching mode.

For high-power fiber laser systems with a long transmission path, the multiple events of discrete mode coupling in the cascade fiber link dominate the deterioration of beam quality M^2. However, due to the information loss in terms of the light field with complex dimensions (e.g., the phase difference or polarization state), the M^2 value is less overt to describe the physical origins of mode degradation[6–8]. From the viewpoint of improving output beam quality, it is an immediate demand to resolve the mode coupling events in the fiber link via accurate determination on not only the modal contents but also the coupling origins. Recent advances in mode decomposition techniques have been reported to precisely interpret the modal content of optical fiber[9–18]. Although these advanced methods are known for their advantages in high-speed measurement or synchronous recognition on multiple field dimensions (e.g., amplitude, polarization or phase), there is still a roadblock for tracing the real origins of mode degradation in the whole fiber path.

Fiber modes are entangled with each other during their propagation. In particular, light propagation in multimode fibers comprises complex intermodal interactions and rich spatiotemporal dynamics[19–22]. The observed fiber output manifests as coherent superpositions of the coupled modes, which, intrinsically, are capable of being traced with a highly

Correspondence to: L. Huang and P. Zhou, College of Advanced Interdisciplinary Studies, National University of Defense Technology, Changsha 410073, China. Emails: hlj203@nudt.edu.cn (L. Huang); zhoupu203@163.com (P. Zhou)

separated degree in the temporal domain. Each eigenmode propagates from the location of coupling origin with an independent group delay, and the total mode delay in the output space is accompanied by accumulation along the propagation distance, that is, the actual fiber length from the mode generation to the emission end. As the mode property that Nicholson *et al.*[23] revealed, this accumulation of mode delay evolves to a specific modulation frequency on the output interference field of several fiber modes under the launching excitation of broadband lasers. Such a technique, known as the spatially and spectrally resolved imaging method[24], is ideally suited for resolving the intermodal dispersion of multimode fibers. While the technique for measuring mode coupling has been thoroughly applied in investigating the single-mode potential or intermodal dispersion of specialty fibers, only a few studies have addressed the tracing mechanism of mode coupling origins in multimode fibers, leaving this field largely unexplored with opportunities to exploit the tracing, monitoring and controlling of beam quality degradation. For fiber laser systems with a cascade fiber link, the interpretation of mode coupling behavior is far more complex. The energy exchanges of different eigenmodes might occur at any splicing points of the fiber link, resulting in mode crosstalk of propagation modes, which is a well-known issue in the subject of high-capacity fiber communications. From the basic perspective of improving beam quality, it is necessary to conduct a full recognition of mode coupling in the cascade fiber link of fiber laser systems that includes not only resolving the modal content, but also tracing the intrinsic origins of mode coupling.

Here we propose a visual method for investigating the origins, evolutions and locations of mode degradation in the fiber delivery system from a physical and controllable perspective. Recent progress in fiber mode analysis has enabled resolving light fields with a surprising speed or a large mode volume, but it is still challenging to nondestructively deduce the origins of mode coupling inside the fiber link only via the output modal contents. For high-power fiber laser systems, a real mode diagnosis concept should have a comprehensive evaluation of modal contents, weights and the physical origins of the high-order modes (HOMs). To demonstrate this concept, a high-power fiber laser delivery system based on passive fibers is established. Through tracing and manipulating the different origins of mode degradation, the independent and synchronous manipulations on both the mode coupling origins and modal weights are realized. Under the bilateral considerations of mode coupling control and a better beam quality factor M^2, the efficient suppression of mode degradation accelerates the enhancement of beam quality M^2 from 1.35 to 1.15. Based on the mode diagnosis strategy in this work, a quantifiable and visual mode control method is fully presented. This work pushes the traditional research of fiber mode analysis aiming at only decomposing the mode contents toward systematic engineering that could construct internal feedback with the practical events of mode coupling. It is a favorable method for us to study the mode behavior in fiber laser systems. More practically, the quest for achieving extreme beam quality becomes a reality by employing this powerful tool.

2. Methodology and experimental strategy

2.1. Analysis of mode coupling origins in the cascade fiber link

To understand the relationships among mode coupling origins, mode degradation and modal contents, one can consider the example of dual-mode excitation in a fiber whose output field is recorded in the temporal domain. For the simplest case, Figure 1(a) shows that the superposition of the LP_{01} and LP_{11} modes is launched into the two-mode fiber #1 as the intended mode. From the launching side to the end of fiber #1, the two modes propagate at their respective mode delays, and arrive at the output end of fiber #1 separately in the temporal domain. At the end of fiber #1, the total delays of the two components, ${\tau_{01}}^{\#1}$ for the LP_{01} mode and ${\tau_{11}}^{\#1}$ for the LP_{11} mode, will achieve their maximum values since they have traveled the full length L_1 of fiber #1, and thus yield the maximum differential mode group delay, ${\tau_{11}}^{\#1} - {\tau_{01}}^{\#1}$. The expression of mode beating between the two mode components is then written as follows:

$$\begin{aligned} I(x,y,z=L,\omega_0+\Delta\omega) = {} & I_{01}|\psi_{01}(x,y)|^2 + I_{11}|\psi_{11}(x,y)|^2 \\ & + 2\,\mathrm{Re}\left\{A_{01}\psi_{01}(x,y)A_{11}^{*}\psi_{11}^{*}(x,y)\right\}\cdot\cos(\Delta\phi) \\ & \cdot\cos\left[\left(\tau_{11}^{\#1}-\tau_{01}^{\#1}\right)\cdot\Delta\omega\right], \end{aligned} \tag{1}$$

in which I and ψ represent the intensity and field distribution, respectively, of eigenmodes at the frequency ω_0 and $\Delta\phi$ refers to the initial phase difference. In this way, the beating frequency determined by the full length L_1 of fiber #1 is ${\tau_{11}}^{\#1} - {\tau_{01}}^{\#1}$. Note that the distributed mode coupling of the two modes can be ignored since the coupling strength in short fibers (several meters) is relatively weak. The propagation of the LP_{01} and LP_{11} modes described in fiber #1 is employed to simulate the discrete mode coupling of this scenario. In this example, the length L_1 of fiber #1 is 10 m. The core diameter and numerical aperture (NA) of fiber #1 are set to 20 μm and 0.06, respectively. To simulate mode beating, the eigenmodes of the fiber at each wavelength point are calculated from 1070 to 1090 nm. The wavelength interval is 0.04 nm, resulting in 501 frames for the LP_{01} and LP_{11} modes. Then, the mode contents of the LP_{01} and LP_{11} modes are assumed to 99% and 1%, respectively. At each wavelength point, the superposed field of the LP_{01} and LP_{11} modes is calculated after propagating over the length L_1. Finally, the mode interference sequence of 501 frames can

https://doi.org/10.1017/hpl.2024.39 Published online by Cambridge University Press

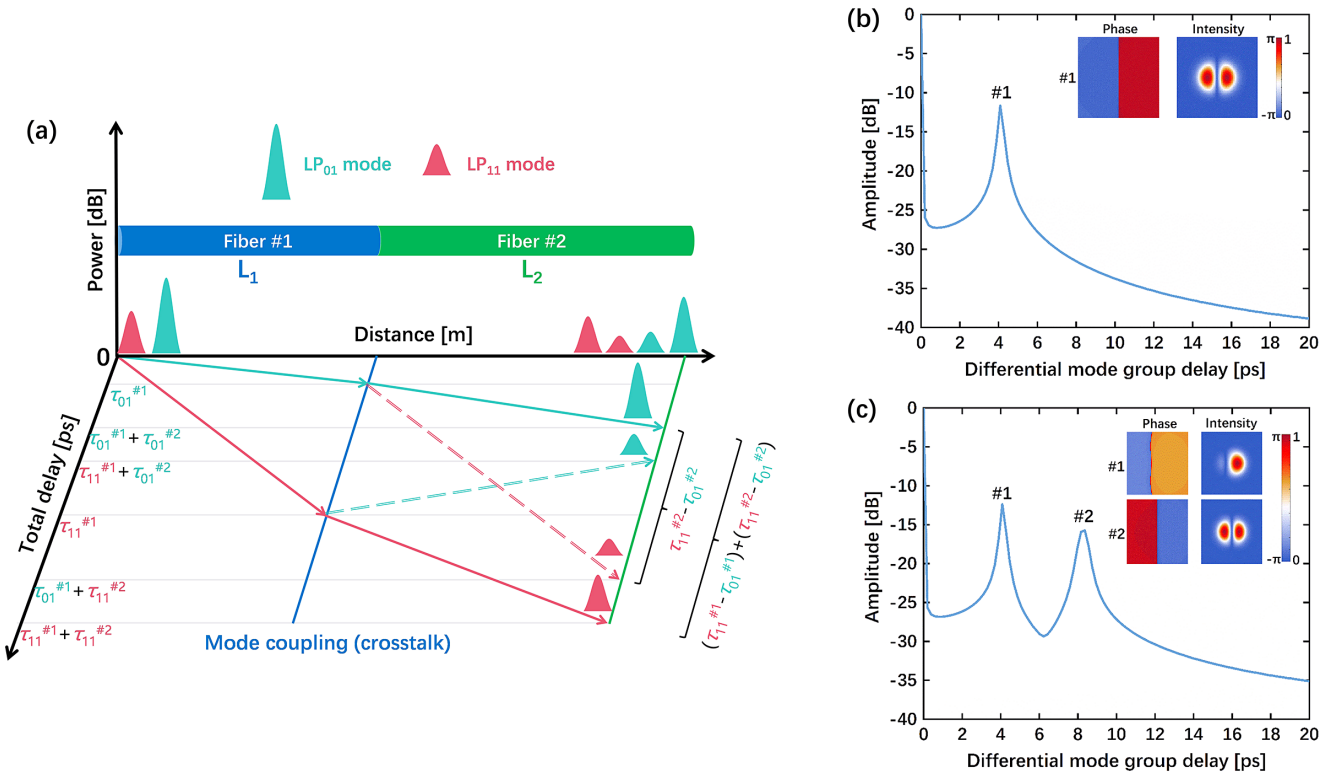

Figure 1. Schematic diagram for explaining the relationships between output mode beating and mode coupling in the cascade fiber link. (a) Mode components generated by the mode crosstalk of fiber splicing, which shows the different origins of high-order modes at the output end. (b) Mode beating frequency for the discrete excitation of the LP_{01} and LP_{11} modes in monolithic fiber. (c) Mode beating frequencies for the cases of the cascade fiber link.

be obtained. Figure 1(b) plots the mode beating trace of two modes, showing the temporal delay position of a discrete peak. As expected, only one event related to the dual-mode excitation at the input end of fiber #1 is observed. The central value of the mode beating frequency is near 4.1 ps, which implies a differential mode group delay of 0.41 ps/m between the LP_{01} and LP_{11} modes.

Extending from the single-stage fiber case, a cascade fiber link that comprises fiber #1 and another piece of fiber, fiber #2, is further considered. Assuming that the two fibers are joined together by a commercial fiber splicer. For simplicity, the length of fiber #2 is set to 10 m. The core diameter and NA of fiber #2 are also set to 20 μm and 0.06, respectively.

In this configuration, the launched modes experience a combined path of L_1 and L_2. The mode crosstalk induced by fiber splicing leads to a new event of mode coupling among eigenmodes. This can be analogized as a single defect of two fibers connected back-to-back at a discrete interface. At this point, the mode crosstalk generates new origins for both the LP_{01} and LP_{11} modes, as illustrated in Figure 1(a). The newly generated mode components propagate discretely with their respective mode delays in fiber #2 while inheriting the accumulated delay in fiber #1. Literally, the LP_{01} mode with the minimum total delay ${\tau_{01}}^{\#1} + {\tau_{01}}^{\#2}$ and the LP_{11} mode with the maximum total delay ${\tau_{11}}^{\#1} + {\tau_{11}}^{\#2}$ are modal components originating from the discrete coupling at the input end of fiber #1, they experience a full accumulation of constant delays and are free of mode crosstalk, and they are called the uncoupled modes. The LP_{01} mode with sub-major total delay ${\tau_{11}}^{\#1} + {\tau_{01}}^{\#2}$ and the LP_{11} mode with sub-minor total delay ${\tau_{01}}^{\#1} + {\tau_{11}}^{\#2}$ experience varied delays disturbed by mode crosstalk, and they are called the coupled modes. Hence, the detected trace at the output end of fiber #2 has four mode components in the temporal domain. Assuming the laser transmission is dominated by the uncoupled LP_{01} mode, two mode beating frequencies in the fiber link could be recognized. The first mode beating between the uncoupled LP_{01} and uncoupled LP_{11} modes is described as follows:

$$\begin{aligned} I(x,y,z=L,\omega_0+\Delta\omega) &= I_{01}|\psi_{01}(x,y)|^2 + I_{11}|\psi_{11}(x,y)|^2 \\ &+ 2\,\mathrm{Re}\left\{A_{01}\psi_{01}(x,y)A_{11}^{*}\psi_{11}^{*}(x,y)\right\}\cdot\cos(\Delta\phi) \\ &\cdot\cos\left\{\left[\left(\tau_{11}^{\#1}-\tau_{01}^{\#1}\right)+\left(\tau_{11}^{\#2}-\tau_{01}^{\#2}\right)\right]\cdot\Delta\omega\right\}. \end{aligned} \tag{2}$$

The second kind of mode beating between the uncoupled LP_{01} and coupled LP_{11} modes is defined as follows:

$$\begin{aligned} I(x,y,z=L,\omega_0+\Delta\omega) &= I_{01}|\psi_{01}(x,y)|^2 + I_{11}|\psi_{11}(x,y)|^2 \\ &+ 2\,\mathrm{Re}\left\{A_{01}\psi_{01}(x,y)A_{11}^{*}\psi_{11}^{*}(x,y)\right\}\cdot\cos(\Delta\phi) \\ &\cdot\cos\left[\left(\tau_{11}^{\#2}-\tau_{01}^{\#2}\right)\cdot\Delta\omega\right]. \end{aligned} \tag{3}$$

https://doi.org/10.1017/hpl.2024.39 Published online by Cambridge University Press

The derivation of mode beating points out a strict correlation between the mode coupling origins and the beating frequencies, which could be separated and analyzed independently by demodulating the beating frequencies of the temporal trace.

However, if the modes have equal values for the total delay, they cannot be separated directly from the temporal trace. To solve this issue, one can determine which HOM dominates the propagation through recognizing them according to the reconstructed profiles for the intensity and the phase. For example, we discuss the specific case when ${\tau_{11}}^{\#1} + {\tau_{01}}^{\#2}$ is equal to ${\tau_{01}}^{\#1} + {\tau_{11}}^{\#2}$. For the mode with the total delay of ${\tau_{11}}^{\#1} + {\tau_{01}}^{\#2}$, its total delay comprises two parts: (1) the delay of the LP_{11} mode in the section L_1 and (2) the delay of the LP_{01} mode in the section L_2. Finally, this propagation trace is emitted from the output end as the LP_{01} mode. This coupling does not degrade the beam quality; instead, it optimizes the modal contents during propagation. For the mode with the total delay of ${\tau_{01}}^{\#1} + {\tau_{11}}^{\#2}$, the propagation trace is emitted from the output end as the LP_{11} mode. This modal component degrades the beam quality, and it is the key factor that needs to be detected and solved in this work. If these two modes co-propagate in the cascade fiber link, they have equal values for the total delay and cannot be distinguished directly. However, based on the mode diagnosis method proposed here, we can resolve the dominated mode through reconstructing the intensity and phase profiles. If the second mode dominates the propagation, the reconstructed profiles show its characteristics since this mode has a stronger beating strength with the fundamental mode. In this case, beam quality degradation occurs. A mode control strategy should be applied to suppress it. In contrast, if the first mode dominates the propagation, mode cleaning is achieved. It is a beneficial effect for beam quality optimization.

This discussion can also be extended to general cases. If multiple modes arrive at the output end of the cascade fiber link with an identical delay, the dominated one has the strongest beating strength with the fundamental mode (at 0 ps). Then, the reconstructed intensity and phase profiles show the characteristics of the dominated HOM. In this way, the main target to optimize the beam quality is suppressing the dominated HOM. Based on the mode diagnosis method proposed here, one can determine the dominated HOM for the specific delay and evaluate the effectiveness of the mode control strategy.

2.2. *Two-mode fiber delivery system and mode diagnosis module*

The prospect for tracing the mode degradation origins yields the construction of the high-power fiber laser delivery system illustrated in Figure 2. In this experimental configuration, a high-power signal laser operating at 1080 nm is transmitted

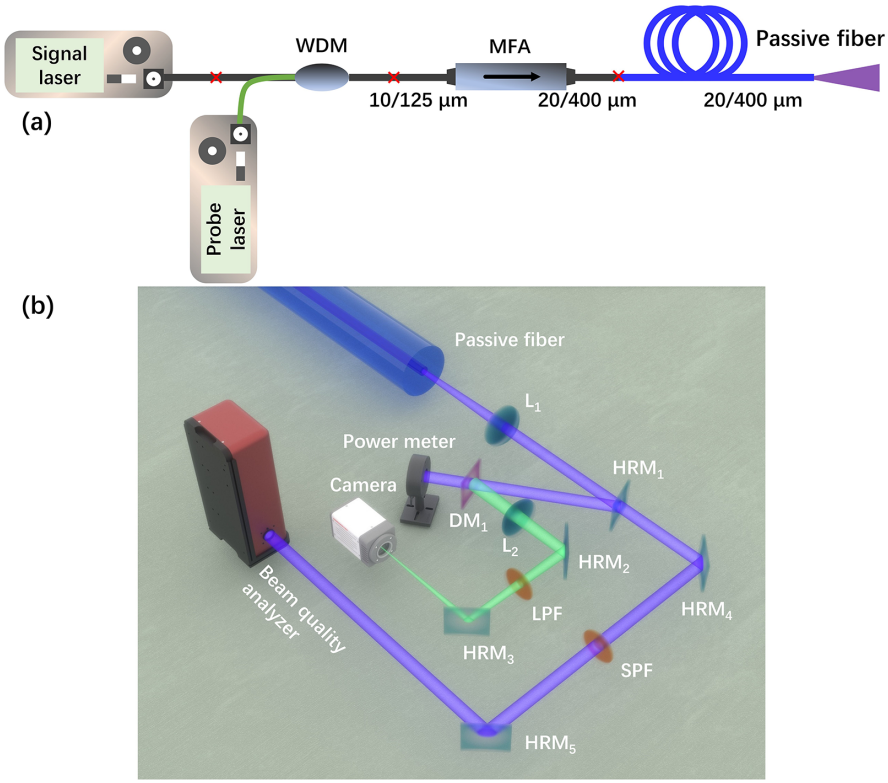

Figure 2. Experimental setup for mode coupling diagnosis in the high-power fiber delivery system. (a) Schematical diagram of the cascade fiber link. (b) Mode diagnosis module for the real-time measurement of beam quality and inner mode coupling.

https://doi.org/10.1017/hpl.2024.39 Published online by Cambridge University Press

by a wavelength division multiplexer (WDM) and a mode field adapter (MFA) firstly, and then delivered through the long-path two-mode passive fiber with the length of near 7 m. The pigtail fiber of the MFA at the output end is near 1.5 m. The core diameter and NA of the MFA fiber pigtail are 20 μm and 0.07, respectively, while the core diameter and NA of the output passive fiber are 20 μm and 0.068, respectively. As shown in Figure 2(a), the probe laser operating at nearly 1120 nm is injected into the delivery system through the WDM synchronously. Note that the fiber pigtails of the signal laser, probe laser and WDM and the input fiber of the MFA are all single-mode fibers. Hence, the signal laser and the probe laser experience almost equivalent mode degradation during the power delivery process if mode coupling behavior exists. The employment of a single-mode signal laser or probe laser prevents the disturbance of the injection modes, which makes the result of mode diagnosis convincing.

The signal laser and probe laser are then launched into the beam diagnosis module, as shown in Figure 2(b). The combined beam of the signal laser and probe laser are collimated by achromatic lens L_1 (effective focal length $f_1 = 50$ mm). The first high-reflection mirror (HRM1) reflects the main power of the laser beam to a dichroic mirror (DM1), which transfers the signal laser to the power meter and reflects the probe laser to achromatic lens L_2 (effective focal length $f_2 = 500$ mm). The combination of achromatic lenses L_1 and L_2 works as a 4*f* system, which magnifies the near field of the output fiber with the magnification of 10×. The second high-reflection mirror (HRM2) and the third high-reflection mirror (HRM3) transmit the magnified beam of the probe laser to a high-speed camera. The pixel depth of the camera is 10 bits. The residual power of the signal laser is further filtered out by a long-pass filter (LPF), guaranteeing a pure probe laser into the camera. In another branch, the sampled beam of the signal laser is reflected to the beam quality analyzer by the fourth high-reflection mirror (HRM4) and the fifth high-reflection mirror (HRM5). Also, a short-pass filter is used to filter out the residual beam of the probe laser. Based on this configuration, online measurement of mode coupling and beam quality could be executed in parallel.

3. Results

3.1. Measurement of beam quality and determination of mode coupling origins

To evaluate the beam quality of the delivery system, all the passive fibers and fiber components are spliced with careful alignment. The result of the output beam quality M^2 is measured as near 1.35, as illustrated in Figure 3(a), indicating that the output profile of the current fiber link deviates from the near-diffraction-limited beam slightly. The definition of the near-diffraction-limited beam is not so explicit; the M^2 of 1.35 could be seen as an excellent output in some instances. However, the aim of this work is chasing extreme beam quality through tracing the mode coupling origins. One can still deduce that significant mode coupling occurs in this fiber link, which, however, could not be traced directly through the M^2 result or any other mode decomposition technique. Both the output fiber and the output fiber of the MFA utilize few-mode fibers, and hence mode degradation may exist at any of the locations or their combination in few-mode fiber link.

The online measurement of mode coupling uses a wavelength slightly larger than the signal wavelength; otherwise, the signal laser and the probe laser could not be well separated for analysis. However, if the wavelength gap between the signal laser and the probe laser is too large, the mode characteristic in the fiber path should be totally discrepant. Before the mode coupling analysis, the key is determining the reasonability of the probe laser. Based on the fiber parameters employed in this experiment (NA = 0.068, core diameter = 20 μm), the normalized frequency, bending loss and effective refractive index at different wavelengths are calculated with the bending radius of 5 cm; the results are illustrated in Figure 3(b). The normalized frequency remains below 3.8 in the range of 1070–1130 nm, which means there is a two-mode state in the whole band. The bending loss of the LP_{11} mode at 1120 or 1130 nm is close to the signal wavelength at 1080 nm; hence they have almost equal modal content measured by the probe laser. The effective refractive index changes smoothly from 1070 to 1130 nm, which prevents the abnormal dispersion of the probe laser compared with the signal laser. Overall, the probe laser selected here is a valid indicator for tracing the mode behavior of the signal laser in this experiment.

Mode analysis is conducted with the probe laser operating at 1120 to 1130 nm firstly. As shown in Figure 3(c), two individual peaks of HOMs are found. The corresponding modal profiles and phase distributions of the two peaks are reconstructed, as shown by the insets of Figure 3(c). The sidelobes of the phase profiles show a difference of π, which provides the evidence for regarding them as LP_{11} modes. The relative contents of dual HOMs, represented by multiple path interference (MPI), are calculated to be –13.9 and –19.9 dB, respectively. MPI is defined as the ratio of powers P_1 and P_2 of the modes, which is expressed as MPI = 10 $\log_{10}$ (P_2/P_1). If the fundamental mode (LP_{01} mode) dominates propagation in the fiber link, the MPI can be calculated by integrating the peak area of an individual HOM[23,24]:

$$\mathrm{MPI} = 10\log_{10}\left[\frac{\iint \mathrm{d}x\mathrm{d}y I_{\mathrm{HOM}}(x,y)}{\iint \mathrm{d}x\mathrm{d}y I_{\mathrm{FM}}(x,y)}\right]. \tag{4}$$

To distinguish the dual HOMs, the first LP_{11} mode with a smaller group delay is labeled as HOM #1, while the

https://doi.org/10.1017/hpl.2024.39 Published online by Cambridge University Press

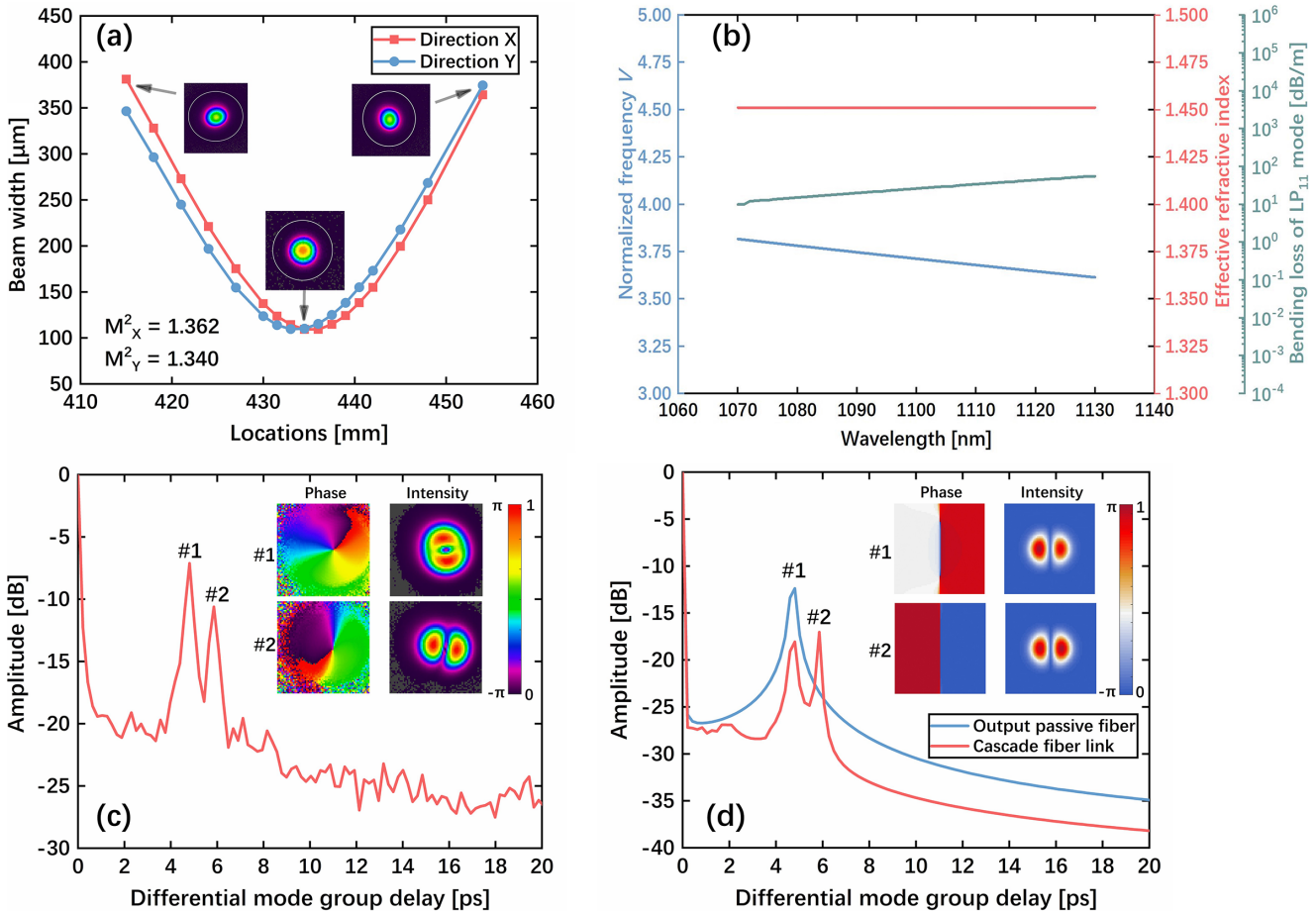

Figure 3. Characterization of the high-power fiber delivery system. (a) Measured beam quality M^2 at the highest transmission power. (b) Theoretical calculations of the output passive fibers for the normalized frequency, effective refractive index and bending loss at different wavelengths. (c) Mode diagnosis for tracing the mode coupling origins in the fiber delivery system. (d) Theoretical calculations of mode beating frequencies for the cases of monolithic fiber and cascade fiber, respectively.

other one is HOM #2. Note that the intensity distributions of the two types of HOMs tend to be orthogonal, and one can subjectively infer that they are caused by the mode mismatch in different directions. Hence, the preliminary results indicate two mode coupling origins in this delivery system. The modal peaks of the HOMs in Figure 3(c) appear as two individual peaks, so both of them originate from discrete mode coupling. In other words, the origins of mode degradation in this fiber link are the two locations of the mode launching points.

For the cascade case discussed in Section 2, the dual peaks of Figure 3(c) mean different origins of mode degradation that should be further clarified. For the case of a monolithic fiber, the excited HOMs travel with a certain group delay (only the two-mode fiber case) with respect to the fundamental mode, leading to a single peak frequency of modal interference. Another origin of mode coupling generates an additional frequency of mode interference due to mode crosstalk. New components of HOMs interfere with the fundamental mode with new differential group delay.

In light of the practical configuration in Figure 2(a), the possible origins of mode degradation should be attributed to the MFA and the output passive fiber or their combination. The total group delay for each mode accumulates with the total delivery length, and this regime yields a strict correlation between the mode coupling within the MFA and the output passive fiber. The first splicing point in Figure 2(a) is the junction point of the single-mode input fiber and the two-mode output fiber within the MFA. At this point, two kinds of fibers are thermally processed for mode field matching. During the fabrication of the MFA, the input single-mode fiber and the output few-mode fiber are thermally processed for mode field adaptation, as the name 'MFA' indicates. Although the adiabatic method for fiber processing maintains mode fidelity in the MFA theoretically, the actual state of fiber splicing in the MFA is not ideal for an absolutely single-mode output. Any inner defect may cause excitation of the unexpected mode and degrade the beam quality. The second splicing point refers to the junction of the MFA pigtail and the output passive fiber. The degradation for

https://doi.org/10.1017/hpl.2024.39 Published online by Cambridge University Press

the splicing of few-mode fibers is a well-known matter for people who devote themselves to mode coupling investigations. The fusion splicing of few-mode fibers proposes thermal expansion of the core elements, which results in inevitable mode mismatching due to the asymmetrical heat applied by splicer electrodes. Hence, the unexpected HOM is excited in the splicing point and degrades the beam quality.

To verify this assumption, the mode coupling conditions of the monolithic fiber and dual fibers are numerically calculated based on the actual fiber parameters, and the results are shown in Figure 3(d). To facilitate the distinguishment of two HOM origins, the theoretical curve of the monolithic fiber is also presented, in which the content of the LP_{11} mode is assumed to be 1%. The length of the monolithic fiber is fixed to 7 m, which is equal to the length of the output passive fiber in Figure 2(a). At the group delay of near 4.6 ps, the modal peak of the LP_{11} mode is reconstructed. This modal peak is associated with the launching excitation of the LP_{11} mode, showing great agreement with the location of HOM #1 in Figure 3(c). After adding another 2-m-length fiber before the monolithic fiber, two separate modal peaks are seen in the so-called cascade fiber when the modal weights of two HOMs are fixed to 0.5% at the same time. The group delays of these two peaks are near 4.6 and 5.8 ps, corresponding to the interference frequency between the dual HOMs and the fundamental mode, respectively. The interference of dual HOMs is negligible for the current HOM weights. The numerical results are in accordance with the mode analysis results in Figure 3(c), providing obvious evidence for tracing the mode coupling origins in the delivery system. The LP_{11} mode with a longer transmission path has a larger accumulation of total group delay. One can conclude that the first HOM peak (HOM #1) originates from the mode coupling in the splicing point between the two fibers, which is associated with the mode mismatching induced by fiber splicing. The second one (HOM #2) refers to the launching excitation of the LP_{11} mode at the beginning end of the cascade fiber, which is related to the inner defect of MFA fabrication. On this basis, the different origins of mode coupling could be manipulated by the individual modal weight or their combinations. Before improving the beam quality M^2 through mode control, more results for tailoring the dual origins of HOMs are presented. For simplicity, the origins of HOM #1 and HOM #2 are assumed as O #1 and O #2, respectively.

3.2. *Precise control of dual HOM origins*

To check the origins of mode coupling in the delivery system, an independent control for each modal peak is carried out. A tight coiling with the bending radius of 3 cm is applied to the output fiber of the MFA firstly. As shown in Figure 4(a), compared with the initial state, the peak amplitude of HOM #2 decreases significantly from –9.5 to –14.3 dB, and MPI #2 decreases from –18.1 to –25.1 dB. The peak amplitude and MPI of HOM #1 remain relatively stable under this condition. Clearly, the tight bending only imposes severe suppression on HOM #2. Hence, the inner defect of the MFA could be completely attributed to the mode coupling origin O #2. As the fundamental mode dominates propagation in the fiber link; the suppression of HOM #2 by tight bending has no obvious effect on the mode interference of the fundamental mode and HOM #1 generation in the subsequent stage. The reconstructed modal profiles of HOM #1 and HOM #2 keep the same orthogonality as the initial state.

After releasing the tight bending near O #2, the output passive fiber is further coiled with a small radius. The bending location is slightly behind the splicing point. Similarly, the mode diagnosis results before and after the coiling are drawn in Figure 4(b) for comparison. Both the peak amplitudes of HOM #1 and HOM #2 are decreasing, indicating the synchronous suppression on both coupling origins. The peak amplitudes of both modal peaks fall from –8.2 and –9.5 dB to –15.7 and –14.7 dB, and the values of MPI vary from –14.8 and –18.1 dB to –29.4 and –26.8 dB, respectively. Tight coiling applied behind the splicing point poses a large bending loss on HOM #1 and HOM #2 simultaneously, which weakens the peak amplitudes of the dual-mode couplings. The mode patterns for mode coupling analysis are captured in the emission space nondestructively, so the mode perturbation affects the peak amplitude of multimode interference.

When we apply tight bending in the first location, only the mode coupling origin O #2 is suppressed. When the tight bending moves to the splicing point, the dual origins of mode coupling are suppressed. Actually, the mode coupling origins of O #1 and O #2 are an objective fact, and tight bending just filters out the HOM content induced by them. The reconstructed modal profiles of HOM #1 and HOM #2 show totally different directionality with respect to the initial state, meaning that the main contents of dual HOMs are suppressed. In fact, misalignment or mode mismatching of fiber splicing occurs in any radial direction. Tight bending in the single direction of the fiber axis has less influence on other directions, and thus the HOMs with different directions become the main content, as shown in Figure 4(b).

Through the tight bending experiment, the controllable manipulation of dual-mode coupling origins is confirmed. Then, all the fibers are released for layout and stress tests. The fiber splicing point of O #1 is rearranged to another spatial location in the optical platform for mode analysis, as shown in Figure 4(c). We tried to prevent the fiber from local tight bending. One can observe that the peak amplitude of HOM #1 falls from –7.1 to –8.2 dB, while HOM #2 remains stable. Mode coupling in the fiber splicing has spatial sensitivity due to the micro-bending imposed by spatial rearrangement. Slight rearrangement of fiber splicing has no obvious effect on the directionalities of the HOMs.

https://doi.org/10.1017/hpl.2024.39 Published online by Cambridge University Press

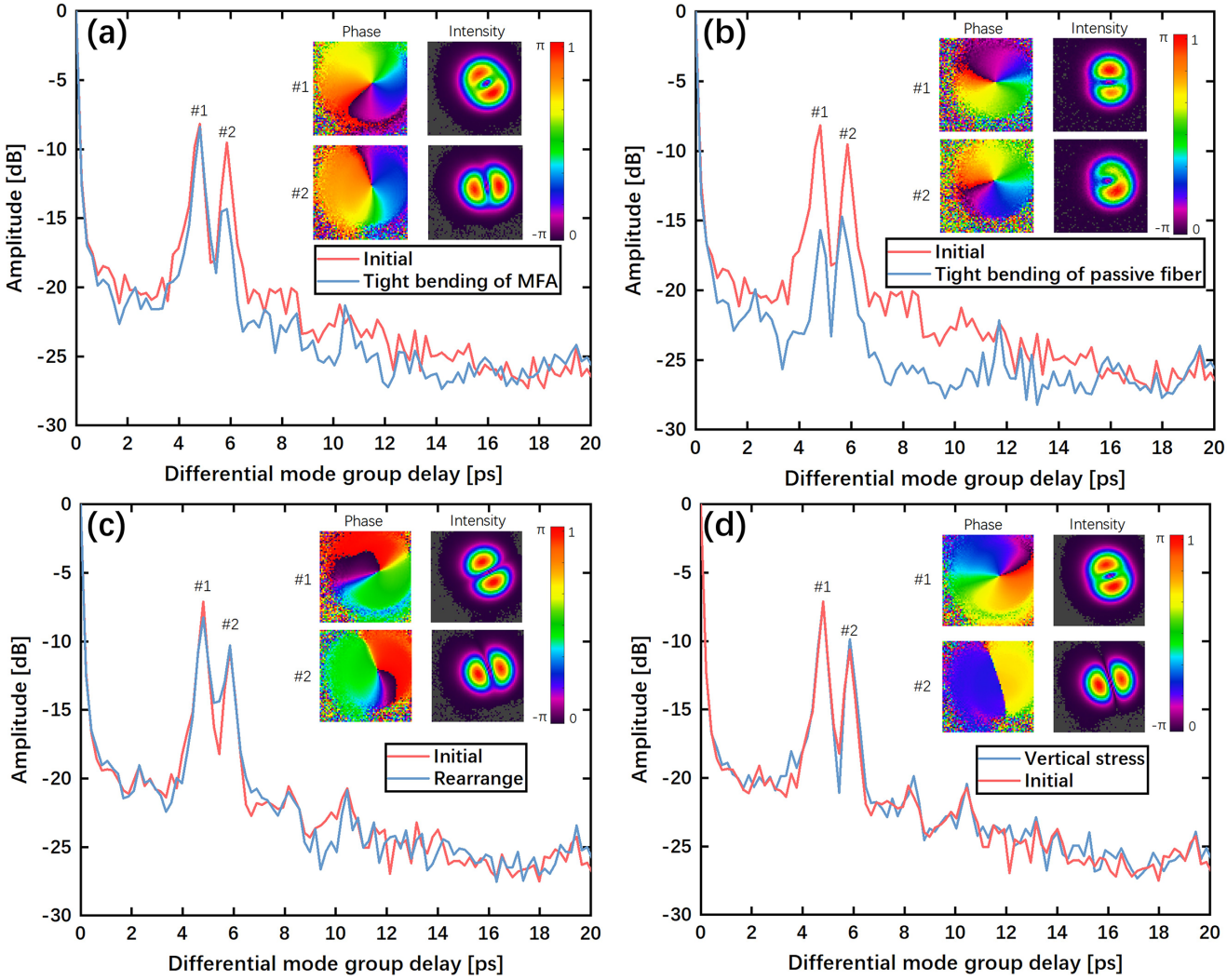

Figure 4. Customized manipulations of the different origins of mode coupling. (a), (b) Mode diagnosis results with tight bending applied on the output pigtail fiber of the MFA or the output passive fiber. (c), (d) Effects of rearrangement or vertical stress on mode coupling origins.

Optical fiber has angular symmetry. The orthogonality of HOM #1 and HOM #2 does not point to the horizontal and vertical directions of the optical platform absolutely. To observe this relationship, mechanical stress is introduced for investigation. Shear stress is applied to the output passive fiber behind the splicing point through a serrated block. Perturbation strength in the vertical direction is adjusted carefully to avoid fiber coating damage. The vertical stress results in an increment of peak amplitude of HOM #2 from –10.6 to –9.8 dB, as illustrated in Figure 4(d). Also. the peak amplitude of HOM #1 has no variation. This phenomenon implies that the vertical stress slightly affects mode coupling origin O #1 while having higher consistency with the spatial direction of HOM #2 induced by mode coupling origin O #2. Thus, the main spatial direction of HOM #1, related to O #1, is parallel to the optical platform. The main spatial direction of HOM #2, related to O #2, is vertical to the optical platform. Considering the reconstructed profiles of the dual HOMs, the orthogonality of the mode pattern can support the inference of mode orientation.

The above results give us a full-dimensional understanding of mode degradation in the fiber delivery system. To conclude, there are two origins of mode coupling. The content of HOM #1, which has a spatial direction parallel to the optical platform, shows an absolute relationship with the inner defect of the MFA, the so-called mode coupling origin O #1. The content of HOM #2, which has a spatial direction vertical to the optical platform, shows an absolute relationship with the mode mismatching of fiber splicing, the so-called mode coupling origin O #2. Based on these findings, the output beam quality M^2 witnesses an unprecedented opportunity for achieving a near-diffraction-limited profile.

3.3. Critical bending condition

Guidance of dual HOMs could be well suppressed through introducing differential bending loss between the fundamental mode and the HOMs. However, tight coiling may cause unexpected loss even for the fundamental mode. The key to fiber coiling is determining the critical bending condition

https://doi.org/10.1017/hpl.2024.39 Published online by Cambridge University Press

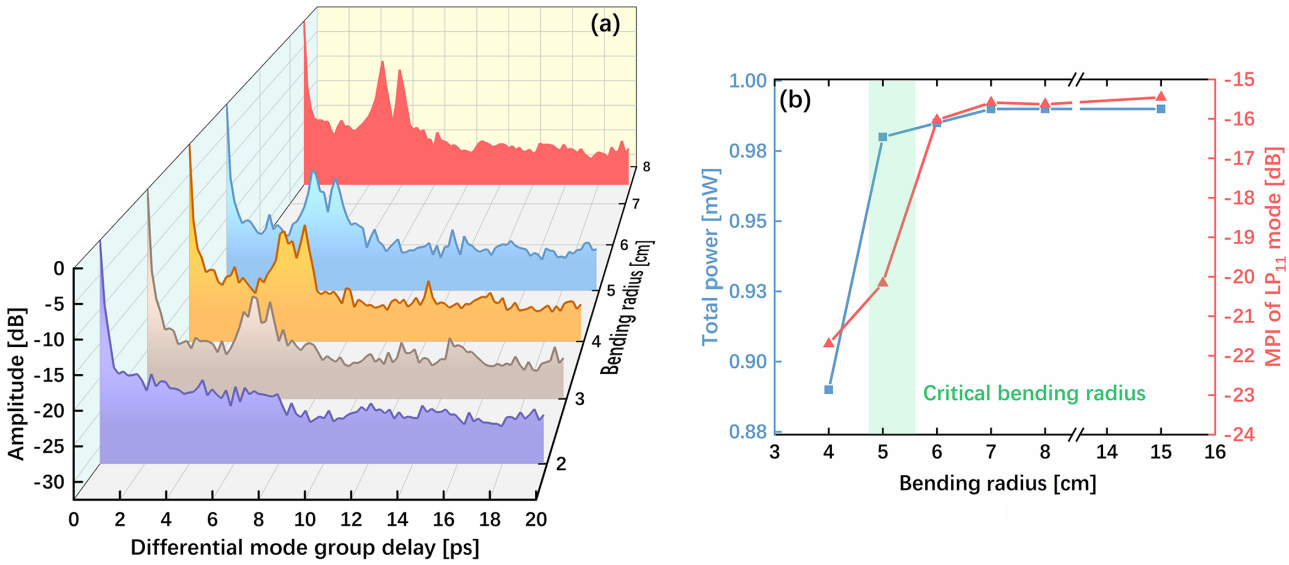

Figure 5. Determination of critical bending condition of the output passive fiber. (a) Mode diagnosis results with different bending radii for the output passive fiber. (b) Power records and MPI evolutions at different bending radii.

for each fiber, through which the tradeoff between strong HOM suppression and high transmission efficiency could be optimized. While many results of fiber lasers with excellent beam quality have been obtained by employing the fiber coiling strategy, only a few studies show a quantizable tool for monitoring the HOM contents related to different mode coupling origins. The pigtail of the MFA and the output passive fiber have different NA values, so the critical bending conditions should be different for them. Owing to the simultaneous suppression on dual HOMs, it is possible to enhance the beam quality by applying critical bending only on the output passive fiber.

The critical bending condition means an optimal bending radius that shows the best suppression on the unexpected HOMs while imposing negligible loss on the fundamental mode, and hence achieving the optimized output beam quality and the highest transmission efficiency. By using the mode diagnosis method developed in this work, we can quantify the suppression ratio of HOMs at different bending radii and determine the critical bending condition by monitoring the total output power simultaneously. Results for mode coupling analysis with varied bending radii of the output passive fiber are plotted in Figure 5(a), which highlight that even a small change of bending radius is enough to see a comparable change in the peak amplitudes of dual HOMs. With the bending radius of 2 cm, one can observe the complete suppression of dual HOMs. However, the bending radius of 2 cm is not moderate enough to ensure a high delivery efficiency. To determine the optimum bending radius, another piece of passive fiber is used for evaluation. It is from the same batch as the output passive fiber in Figure 2(a), and its length is 4 m. To achieve substantial LP_{11} excitation, the single-mode fiber (pigtail of the laser source) and passive fiber are intentionally spliced with a core misalignment of 2 μm. A single coil with a progressively smaller diameter is applied at 0.5 m from the splicing point. For each bending case, both the MPI of the LP_{11} mode and total transmitted power are recorded. The fiber exhibits robust power confinement at the radius over 6 cm, and the MPI of LP_{11} is irrelevant to the variation of bending radius in this range. A main principle for us is exploring the optimum radius at which the fiber has efficient suppression on the LP_{11} mode but negligible loss of the fundamental mode. One can clearly realize that there is a highest-yielding point at the bending radius of 5 cm, where the MPI of the LP_{11} mode experiences a decrement over 4 dB (from –16.0 to –20.2 dB) for a single coil. Meanwhile, the total transmitted power retains a moderate loss, which is mainly attributed to the loss of the LP_{11} mode. This quantitative result combined with the mode diagnosis in Figure 5(a) yields an optimum bending radius for suppressing the HOMs generated by mode coupling. In this way, the critical bending condition, that is, the bending radius of 5 cm, is determined.

After applying 10 coils of critical bending radius on the output passive fiber, the measured M^2 drops to near 1.15 at the highest delivery power of 315 W, as illustrated in Figure 6(a). The maximum power of the delivery system is limited by the power handling capacity of the WDM. Further analysis of dual-mode coupling origins shows that the peak amplitudes of dual HOMs are well restrained, as shown in Figure 6(b). The MPIs of HOM #1 and HOM #2 are estimated to be –30.0 and –41.4 dB, respectively. The comparison of M^2 and HOM contents before and after mode control is summarized in Table 1, from which the goal of extreme beam quality is realized. The output powers before and after mode diagnosis are drawn in Figure 6(c), from

https://doi.org/10.1017/hpl.2024.39 Published online by Cambridge University Press

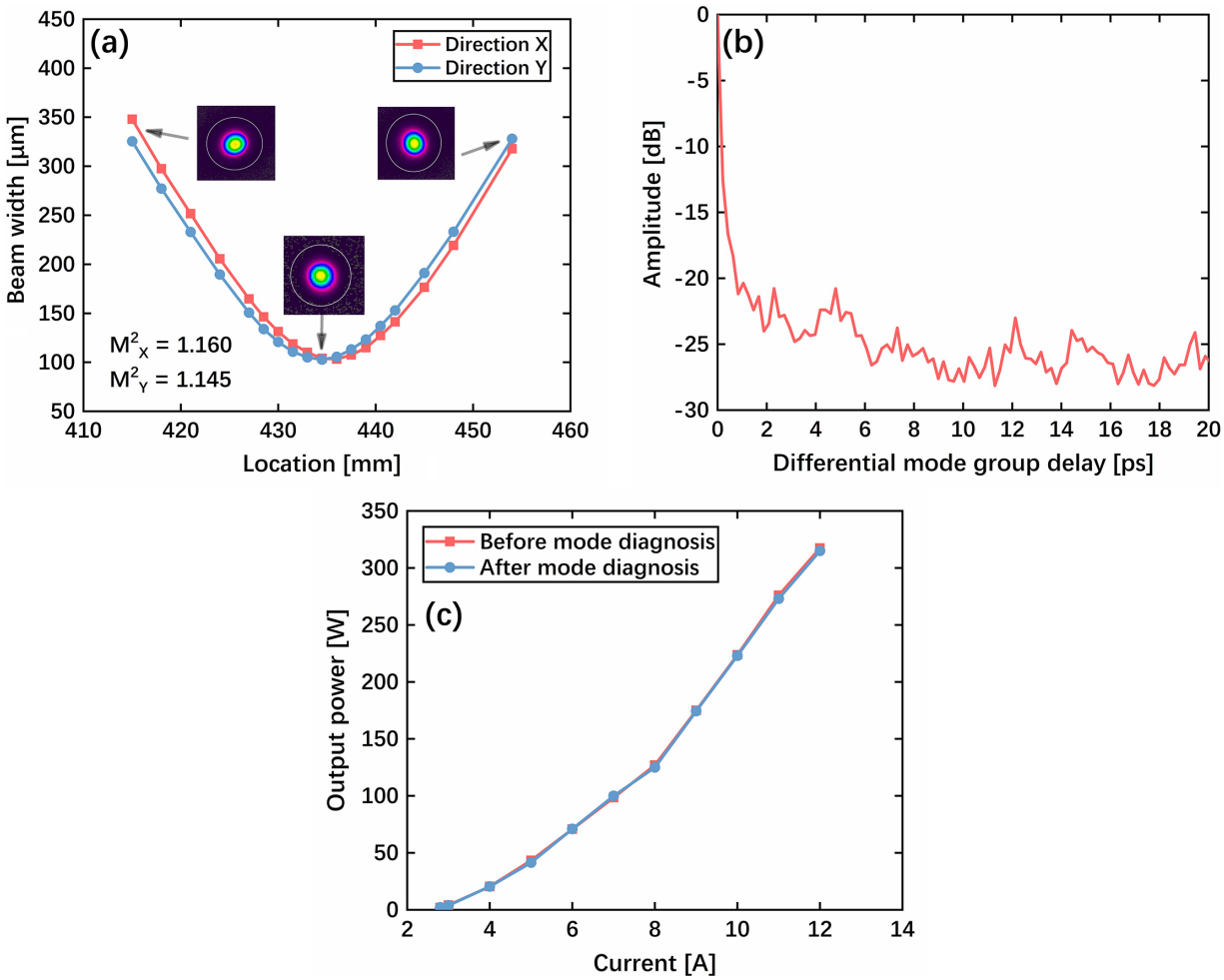

Figure 6. Output properties of the high-power delivery system. (a) Beam quality factor M^2 measured at the output space. (b) Mode diagnosis results with the critical bending of 10 coils applied on the output passive fiber. (c) Power evolutions of the output laser before and after mode diagnosis.

Table 1. Comparison of M^2 results and HOM contents before and after mode control instructed by tracing the mode coupling origins.

	Before mode diagnosis	After mode diagnosis
Beam quality M^2	1.35	1.15
Content of HOM #1	–13.9 dB	–30.0 dB
Content of HOM #2	–19.9 dB	–41.4 dB
Output power	318 W	315 W

which the tendency of power evolution shows negligible loss of the signal laser. One can conclude that the high efficiency of an almost strict single-mode laser is achieved based on the mode diagnosis technique.

4. Discussion and conclusion

Fiber coiling, the strategy used here for suppressing the HOM contents, is essentially a passive method for mode control in the fiber link. In some situations, a coiling diameter of less than 20 cm is not acceptable for fiber delivery applications that require loose coiling. Actually, the suppression of mode coupling should be developed to a more intrinsic strategy that fundamentally reduces the strength of mode coupling origins. For instance, the inner defect of the MFA can be eliminated during the fabrication process. Considering the method for analyzing mode coupling proposed in this work, the online optimization of fiber device fabrication is realizable. It is possible to get an ideal fiber device through optimizing the individual parameters of the thermal process step by step, in which the method for mode coupling analysis in the cascade fiber link provides a quantitative diagnosis for us to monitor the fabrication of fiber devices. In a similar way, the optimized parameters with the lowest mode coupling are also achievable for fiber splicing.

The issue for pursuing extreme beam quality should be also discussed. Through tracing and manipulating the dual-mode coupling origins, the mode diagnosis result indicates almost complete suppression of dual HOMs. However, the measured M^2 of 1.15 does not match the general perception of the extreme beam quality ($M^2 \sim 1.0$). To enable the online

https://doi.org/10.1017/hpl.2024.39 Published online by Cambridge University Press

analysis of the mode property we employ a longer waveband for the probe laser compared with the signal wavelength and, in this way, the bending loss of the LP_{11} mode is relatively higher for the probe laser even though the calculation results in Figure 3(b) show a difference between the signal laser and the probe laser. It should be emphasized that there is still a small amount of LP_{11} content at the signal wavelength. Even the level near –30 dB of HOMs may result in the increment of M^2[25]. In Figure 3(b), when the bending radius is 5 cm, the bending losses of the LP_{11} mode at 1080, 1120 and 1130 nm are calculated to be 15, 44 and 54 dB/m, respectively. Such a difference of bending loss between the probe laser and the signal laser impedes the pursuit of achieving extreme beam quality. Although the mode diagnosis results suggest the complete suppression of HOMs, the guided modes at the signal wavelength still have nonnegligible HOM content. Ideally, the supported mode number and the bending loss of the laser fiber should have same values for the signal waveband and the probe waveband. If the wavelength of the probe laser is too long, the HOM may experience much higher bending loss than the signal laser, resulting in a deceptive conclusion in evaluating the single-mode performance. To obtain a value of M^2 closer to 1.0, one can adopt a shorter waveband for the probe laser, but this setting poses a higher demand on the filtering band of the beam splitter. As an example, one can utilize the configuration of 1080/1090 nm for the signal laser and the probe laser, respectively, to conduct the mode coupling analysis. This strategy is especially suitable for narrow-linewidth fiber laser systems, which will take a step toward reality in our future work.

In conclusion, the present work demonstrates a powerful approach to suppress the mode degradation in a high-power fiber delivery system through tracing and manipulating the mode coupling origins in the cascade fiber link. Theoretical simulation and experimental results show that resolving the mode beating frequencies within the fiber link enables unprecedented manipulation of the independent origins of mode coupling or their combination. Using this feature, a two-mode fiber delivery system is constructed for verification, and the results of measured M^2 values experience a significant optimization from 1.35 to 1.15 at the highest power of over 300 W. Despite the enhancement of beam quality M^2, the overall delivery efficiency remains stable owing to the precise determination of the critical bending condition, through which both the HOM suppression and the transmission efficiency are maintained.

How to mitigate the degradation of beam quality is a key subject for high-power fiber laser facilities. The beam quality of fiber lasers is essentially determined by the modal contents of the output field, which shows an intrinsic correlation with the behavior of mode coupling within optical fibers, especially for laser systems with an all-fiber format. The configuration of a fiber laser system comprises many kinds of fibers and fiber devices, which establish a cascade fiber link for laser transmission. Mode coupling may happen at any point, section or their combinations in the fiber link, resulting in the overall degradation of output beam quality. Hence, the key issue for improving beam quality is clarifying the real origins of mode coupling. This work pushes the traditional research of fiber mode analysis aiming at only decomposing the mode contents toward systematic engineering that could construct internal feedback with the practical events of mode coupling. This technique unlocks the internal correlations between mode degradation and mode coupling origins in the cascade fiber link, and opens up a prospective path to seek extreme beam quality in high-power fiber laser systems.

Acknowledgements

This work was supported by the National Key Research and Development Program of China (No. 2022YFB3606000), the National Natural Science Foundation of China (Nos. 12174445 and 62061136013) and the State Key Laboratory of Pulsed Power Laser Technology (No. SKL2021ZR06).

References

1. C. N. Danson, C. Haefner, J. Bromage, T. Butcher, J.-C. F. Chanteloup, E. A. Chowdhury, A. Galvanauskas, L. A. Gizzi, J. Hein, D. I. Hillier, N. W. Hopps, Y. Kato, E. A. Khazanov, R. Kodama, G. Korn, R. Li, Y. Li, J. Limpert, J. Ma, C. H. Nam, D. Neely, D. Papadopoulos, R. R. Penman, L. Qian, J. J. Rocca, A. A. Shaykin, C. W. Siders, C. Spindloe, S. Szatmári, R. M. G. M. Trines, J. Zhu, P. Zhu, and J. D. Zuegel, High Power Laser Sci. Eng. **7**, e54 (2019).
2. C. Jauregui, J. Limpert, and A. Tünnermann, Nat. Photonics **7**, 861 (2013).
3. J. Zuo and X. Lin, Laser Photonics Rev. **16**, 2100741 (2022).
4. X. Chen, T. Yao, L. Huang, Y. An, H. Wu, Z. Pan, and P. Zhou, Adv. Fiber Mater. **5**, 59 (2023).
5. Y. Wang, G. Chen, and J. Li, High Power Laser Sci. Eng. **6**, e40 (2018).
6. H. Yoda, P. Polynkin, and M. Mansuripur, J. Lightwave Technol. **24**, 1350 (2006).
7. S. Wielandy, Opt. Express **15**, 15402 (2007).
8. R. Tao, L. Huang, P. Zhou, L. Si, and Z. Liu, Photonics Res. **3**, 192 (2015).
9. M. Jiang, H. Wu, Y. An, T. Hou, Q. Chang, L. Huang, J. Li, R. Su, and P. Zhou, PhotoniX **3**, 16 (2022).
10. D. Flamm, C. Schulze, D. Naidoo, S. Schroter, A. Forbes, and M. Duparre, J. Lightwave Technol. **31**, 1023 (2013).
11. L. J. Huang, S. F. Guo, J. Y. Leng, H. B. Lu, P. Zhou, and X. A. Cheng, Opt Express **23**, 4620 (2015).
12. Z. Liu, S. Yan, H. Liu, and X. Chen, Phys. Rev. Lett. **123**, 183902 (2019).
13. E. S. Manuylovich, V. V. Dvoyrin, and S. K. Turitsyn, Nat. Commun. **11**, 5507 (2020).
14. X. Wei, J. C. Jing, Y. Shen, and L. V. Wang, Light Sci. Appl. **9**, 149 (2020).
15. B. Kim, J. Na, J. Kim, H. Kim, and Y. Jeong, Opt. Express **29**, 21502 (2021).
16. Y. Liu, Q. Liu, J. Xiong, S. Zhao, M. Lyu, X. Pan, J. Zhang, and Z. He, Opt. Lett. **47**, 5813 (2022).

https://doi.org/10.1017/hpl.2024.39 Published online by Cambridge University Press

17. Q. Zhang, S. Rothe, N. Koukourakis, and J. Czarske, APL Photonics **7**, 066104 (2022).
18. Y. An, L. Huang, J. Li, J. Leng, L. Yang, and P. Zhou, Opt. Express **27**, 10127 (2019).
19. O. Tzang, A. M. Caravaca-Aguirre, K. Wagner, and R. Piestun, Nat. Photonics **12**, 368 (2018).
20. D. Cruz-Delgado, S. Yerolatsitis, N. K. Fontaine, D. N. Christodoulides, R. Amezcua-Correa, and M. A. Bandres, Nat. Photonics **16**, 686 (2022).
21. L. G. Wright, F. O. Wu, D. N. Christodoulides, and F. W. Wise, Nat. Phys. **18**, 1018 (2022).
22. H. Wu, H. Li, Y. An, R. Li, X. Chen, H. Xiao, L. Huang, H. Yang, Z. Yan, J. Leng, Z. Pan, and P. Zhou, High Power Laser Sci. Eng. **10**, e44 (2022).
23. J. W. Nicholson, A. D. Yablon, S. Ramachandran, and S. Ghalmi, Opt. Express **16**, 7233 (2008).
24. J. W. Nicholson, A. D. Yablon, J. M. Fini, and M. D. Mermelstein, IEEE J. Select. Top. Quantum Electron. **15**, 61 (2009).
25. F. Amrani, J. H. Osório, F. Delahaye, F. Giovanardi, L. Vincetti, B. Debord, F. Gérôme, and F. Benabid, Light Sci. Appl. **10**, 7 (2021).

https://doi.org/10.1017/hpl.2024.39 Published online by Cambridge University Press